Eur Biophys J (1996) 25: 139–150 © Springer-Verlag 1996

ARTICLE

P. Mitton · M. S. P. Sansom

Molecular dynamics simulations of ion channels formed by bundles of amphipathic α-helical peptides

Received: 23 April 1996 / Accepted: 7 August 1996

Abstract Ion channels may be formed by self-assembly of amphipathic α-helical peptides into parallel helix bundles. The transbilayer pores formed by such peptides contain extended columns of water molecules, the properties of which may differ from those of water in its bulk state. The de novo designed peptides of DeGrado et al., which contain only leucine and serine residues, are considered as a simple example of such channels. Molecular dynamics simulations of peptide helix bundles with water molecules within and at the mouths of their pores are used to refine such models and to investigate the properties of intra-pore water. The translational and rotational mobility of water molecules within the pores are reduced relative to bulk water. Furthermore, intra-pore waters orient themselves with their dipoles anti-parallel to the helix dipoles, as do the hydroxyl groups of serine residues. Comparison of approximate predictions of ionic conductances with experimental values provides support for the validity of these models.

Key words Ion channel · Water · Molecular dynamics · Dipole · α-helix · Peptide

Introduction

Transbilayer pores are present in ion channels (Unwin 1989; Hille 1992), in bacterial porins (Cowan et al. 1992), and in related transport proteins e. g. aquaporins (Engel et al. 1994; Walz et al. 1995). The transmembrane segments of these integral membrane proteins are believed to surround a central pore which contains multiple water molecules (Kreusch and Schulz 1994; Unwin 1995). In order to understand the molecular basis of transport through transbilayer pores it is necessary to understand the physical properties of such intra-pore water (Dani and Levitt 1990; Karshikoff et al. 1994).

In several classes of ion channels the central pore is formed by a bundle of parallel α-helices. Examples of channels exhibiting this structural motif include the nicotinic acetylcholine receptor (Unwin 1993; Unwin 1995; Sankararamakrishnan et al. 1996), phospholamban (Adams et al. 1995; Arkin et al. 1995), influenza M2 protein (Sansom and Kerr 1993), and several channel-forming peptides (CFPs) (Sansom 1991). CFPs are amphipathic α-helical peptides which self-assemble within lipid bilayers, in response to a transbilayer voltage difference, to form ion permeable pores. Such CFPs include antibiotics e. g. alamethicin (Sansom 1993a, b) and toxins e. g. *Staphylococcus aureus* δ-toxin (Mellor et al. 1988; Kerr et al. 1995; Kerr et al. 1996). Furthermore, certain *de novo* designed synthetic peptides also act as CFPs (Lear et al. 1988; DeGrado and Lear 1990; Chung et al. 1992; Åkerfeldt et al. 1993; Kienker et al. 1994; Lear et al. 1994). The helix bundles formed by CFPs are dynamic assemblies. Channels containing different numbers of helices per bundle may be formed by the same peptide species. CFPs have been employed as elements of synthetic helix bundles by covalent tethering to a rigid or semi-rigid template (Montal 1990; Åkerfeldt et al. 1992; Montal 1995; You et al. 1996) in order to create channels with a restricted or fixed number of constituent helices. In the absence of a high resolution crystallographic structure for a helix bundle channel, molecular modelling studies have been widely employed in order to understand the molecular basis of ion channel function in these systems (Lear et al. 1988; Oiki et al. 1990; Raghunathan et al. 1990; Åkerfeldt et al. 1993; Kerr et al. 1994; Lear et al. 1994; Adams et al. 1995; Montal 1995; Sankararamakrishnan and Sansom 1995; Sansom et al. 1995; Kerr et al. 1996; Sankararamakrishnan et al. 1996).

The *de novo* designed synthetic CFPs of DeGrado and colleagues (Lear et al. 1988; Åkerfeldt et al. 1993) are an attractive system for modelling and simulation studies, as they combine relative structural simplicity with a func-

P. Mitton · M. S. P. Sansom (✉)
Laboratory of Molecular Biophysics, The Rex Richards Building, University of Oxford, South Parks Road, Oxford, OX1 3QU, UK
(Fax: +44 1865-51 04 54, e-mail: mark@biop.ox.ac.uk)

tional complexity comparable to that observed in other channel systems. Previous modelling studies (Lear et al. 1988; Åkerfeldt et al. 1993; Kerr et al. 1994) have shown that helix bundles formed by these CFPs prefer to adopt a left-handed supercoiled conformation. The internal diameters of these helix bundle models are consistent with the conductance and selectivity properties of the corresponding channels. In this paper we use molecular dynamics (MD) simulations, in the presence of explicit water molecules, to refine such models. We analyze the structure and dynamics of water molecules within the resultant pores. Comparison of the results with those from comparable channel simulations (Chiu et al. 1991; Roux and Karplus 1994; Engels et al. 1995; Breed et al. 1996) suggest properties of intra-pore water which may be common to many ion channels. For the *de novo* CFPs in particular, it seems that within pores formed by bundles of parallel α-helices water molecules are significantly immobilized, and that water and sidechain hydroxyl dipoles are preferentially aligned relative to the pore axis.

Methods

General

Initial models were generated using XPLOR (Brünger 1992) version 3.1. MD simulations were performed using CHARMM (Brooks et al. 1983) version 23f3. Simulations were run on a DEC2100. All other calculations were carried out on Silicon Graphics R3000 and R4000 workstations. Structures were manipulated and examined using Quanta V4.0 (Biosym/Molecular Simulations), and diagrams were drawn using Quanta or Molscript (Kraulis 1991).

Generation of initial models of pores

Initial models of pores were generated using simulated annealing via restrained molecular dynamics (SA/MD), as described in previous publications (Kerr et al. 1994; Sansom and Kerr 1995). Details of individual models are provided below. From each ensemble of 25 structures generated by SA/MD, that with the highest degree of rotational symmetry was used for solvation and MD simulations. Extended atoms were used, i. e. only polar hydrogen atoms were explicitly represented.

Solvation of models and MD simulations

Pore models were solvated and MD simulations performed using protocols based on those described in Breed et al. (1996). The water model employed was a TIP3P three-site model (Jorgensen et al. 1983) with partial charges $q_o = -0.834$ and $q_H = +0.417$, modified as in the PARAM19 parameter set of CHARMM to allow internal flexibility of the water molecules, as described by Venable et al. (1993). Model pores were solvated using a pre-equilibrated cylinder (length = 60 Å, radius = 7 Å) of water molecules. Water molecules from this cylinder were selected so that the central pore and the cap regions at either mouth of the pore were solvated, but such that no water molecules were present on the bilayer-exposed faces of the pores.

Solvated model pores were energy minimized prior to MD simulations. A four-stage energy minimization was performed: (a) 1000 cycles of adopted basis Newton Raphson (ABNR) minimization with the protein atoms fixed; (b) 1000 cycles of ABNR with the protein backbone atoms restrained; (c) 1000 cycles of ABNR with weak restraints on the protein Cα atoms only; and (d) 1000 cycles of ABNR with no positional restraints. During MD simulations restraints were applied or water molecules, in order to guard against 'evaporation' from the caps at either mouth of the pore. The form of the restraining potential, applied to the waters using the MMFP module of CHARMM, was:

$$E = \frac{F}{2}\exp\left(-\frac{\Delta}{\lambda}\right) \qquad \text{if } \Delta > 0 \tag{1}$$

or:

$$E = F\left[1 - \frac{1}{2}\exp\left(+\frac{\Delta}{\lambda}\right)\right] \qquad \text{if } \Delta \le 0 \tag{2}$$

where $F = -7.5$ kcal/mol and $\lambda = 0.25$ Å, and in which $\Delta = r - r_{WALL}$, i. e. the distance of the atom from the restraining "wall". Note that Eq. (1) applies to water atoms outside the wall and Eq. (2) applies to water atoms inside the wall. The restraining wall was cylindrical in shape, with length 60 Å and radius 7 Å (models IN4 and PN4), 9 Å (model *IN5*) or 9.5 Å (model *IN6*).

MD simulations used a 1 fs timestep. The system was heated from 0 to 300 K in 6 ps (5 K, 0.1 ps steps) and equilibrated for 9 ps at 300 K by rescaling of atomic velocities every 0.1 ps. The production stage of the simulation was for 85 ps, giving a total simulation time of 100 ps. Dynamic properties of water were analyzed over the 170 coordinate set trajectories, which were saved every 0.5 ps during the production stage of the simulations. Non-bonded interactions (both electrostatic and van der Waals) between distant atoms were truncated using a shift function (Brooks et al. 1983) with a cutoff of 13.0 Å, and a fixed dielectric of $\varepsilon = 1$ was used for electrostatic interactions. In simulation *IN6** the simulation *IN6* was repeated, but with the SHAKE option of CHARMM used to maintain fixed bond lengths and to hold the TIP3P water molecules rigid.

Analysis

Two parameters characteristic the dynamic behaviour of water molecules were estimated: the self-diffusion coefficient, D (which measures translational mobility), and the rotational reorientation rate time, τ_2^{-1}. The self-diffusion coefficient for each water molecule was obtained by evaluation of its mean square displacement as a function of

time:

$$\langle r(t)^2\rangle) = \langle (r(t) - r(0))\rangle^2 \quad (3)$$

using the relationship:

$$\lim_{t\to\infty}\langle r(t)^2\rangle = 6Dt + c \quad (4)$$

to fit the $\langle r(t)^2\rangle$ data for $t = 3$ to 6 ps. Inspection of $\langle r(t)^2\rangle$ vs. t curves for individual waters revealed them to approach linearity within this region. A second order rotational correlation function (Rossky and Karplus 1979) was defined in terms of the angle, $\theta(t)$, made by the dipole of a water molecule at time 0 and the dipole of the same water molecular at time t:

$$C_2(t) = \langle (3\cos^2\theta(t) - 1)/2\rangle \; . \quad (5)$$

For each water molecule this function was fitted (for the regions from 0.5 to 5.0 ps) as a mono-exponential decay with time constant τ_2. Inspection of plots of $C_2(t)$ for individual waters provided support for the fitting of a mono-exponential to these data. A rotational reorientation rate (τ_2^{-1}) was calculated as the reciprocals of the fitted time constant.

Water dipole orientations were analyzed for the final ($t = 100$ ps) coordinate sets. The orientation of water molecules relative to the pore (z) axis was measured in terms of the projection onto the z axis of the dipole moment of each water, μ_z. Note that for an ideal TIP3P water molecule with its dipole exactly parallel to the z axis, $\mu_z = 2.35$ Debye. The pore axis (z) runs from the N-termini to the C-termini of the helices. Thus, a water molecule with its O atom closer to the N-termini and its H atoms closer to the C-termini would have a positive value for μ_z.

The pore/water interaction energy of the models was defined as $\Delta E_{PW} = E\ (pore + water) - E\ (pore) - E\ (water)$. The interaction energy between the helices making up the pore was defined as $\Delta E_{HH} = E(pore) - E(isolated\ helices)$.

Pore radius profiles were measured using HOLE (Smart et al. 1993), which calculates the pore radius as a function of distance along the pore (z) axis. Pore radius profiles were used to estimate an upper bound on the ionic conductance for a given model (Sansom and Kerr 1995). This was obtained by approximating a transbilayer pore as a cylinder of radius $r(z)$ (given by HOLE) filled with salt solution of resistivity ρ. If a pore runs from $z = a$ to $z = b$, then its overall electrical resistance is $R = R_a + R_{PORE} + R_b$, where R_a and R_b are the access resistances at either mouth of the pore (Hille 1992) and where R_{PORE} is the resistance of the pore *per se*, obtained by integrating $\rho/(\pi r^2)$ along the length of the pore (Kuyucak and Chung 1994). Thus, the upper bound on the conductance is given by the reciprocal of R, i. e.:

$$G_{UPPER} = \left[\frac{\rho}{4r_a} + \int_a^b \frac{\rho}{\pi r^2}\,dz + \frac{\rho}{4r_b}\right]^{-1} .$$

Values of G_{UPPER} were calculated using $\rho = 0.13\ \Omega$m, equivalent to the resistivity of 0.5 M KCl.

Results

Definition of models

The model pores used in these simulations are defined in Table 1. As shown by DeGrado and colleagues (Lear et al. 1988; DeGrado and Lear 1990; Åkerfeldt et al. 1992; Åkerfeldt et al. 1993; Lear et al. 1994), the peptide $(LSSLLSL)_3NH_2$ forms monovalent cation selective ion channels, with a single channel conductance ($G = 70$ pS in 0.5 M KCl) and a cutoff radius (ca. 4 Å) consistent with channels formed by hexameric, and possibly also pentameric, bundles of helices. Models *IN6* and *IN5* correspond to such assemblies of this peptide. In contrast, peptide $(LSLLLSL)_3NH_2$ forms proton selective channels which do not support permeation of monovalent cations larger than H^+. This suggests that the channel is formed by a tetrameric helix bundle, as in model *PN4*. Model *IN4* was generated to enable comparison of the properties of tetrameric assemblies of the two peptide sequences.

In all cases the bundles are formed from approximately parallel (rather than antiparallel) helices. This is supported by the asymmetry of channel formation in response to a *cis* negative voltage applied across a bilayer (Lear et al. 1988) and by the rectification properties of the channels thus formed (Kienker et al. 1994). The helices within each bundle are oriented such that the serine sidechains point inwards towards the pore lumen, and the leucine sidechains point outwards. As expected, the number of water molecules required to solvate each model, within and at the mouths of the pore, increases as the number of helices increases. Less obviously, significantly more waters were required to solvate model *PN4* than model *IN4* (see below).

Models *IN5* and *IN6*

Snapshots of models *IN5* and *IN6*, taken at the end of the $t = 100$ ps MD trajectory, are shown in Fig. 1. From these

Table 1 Definition of models

Model	Sequence	Number of helices	Number of waters	Number of atoms
IN4	$(L\text{-}S\text{-}S\text{-}L\text{-}L\text{-}S\text{-}L)_3\text{-}NH_2$	4	103	1049
IN5	$(L\text{-}S\text{-}S\text{-}L\text{-}L\text{-}S\text{-}L)_3\text{-}NH_2$	5	209	1552
IN6	$(L\text{-}S\text{-}S\text{-}L\text{-}L\text{-}S\text{-}L)_3\text{-}NH_2$	6	256	1875
PN4	$(L\text{-}S\text{-}L\text{-}L\text{-}S\text{-}L)_3\text{-}NH_2$	4	145	1187

Table 2 Geometric and energetic properties

Model	$\langle\Omega\rangle$ (°)	$\langle D\rangle$ (Å)	$\langle R^{PORE}\rangle$ (Å)	R_{MIN} (Å)	ΔE_{HH}^{VDW} (kcal/mol)	E_{HH}^{ELEC} (kcal/mol)	ΔE_{PW}^{VDW} (kcal/mol)	ΔE_{PW}^{ELEC} (kcal/mol)
IN4	+23.5 (±7.7)	8.3 (±0.6)	1.5 (±0.3)	0.97	–147	–15	–53	–972
IN5	+13.2 (±3.6)	9.3 (±0.7)	2.5 (±0.6)	1.6	–145	+112	–156	–1767
IN6	+10.7 (±5.0)	9.4 (±0.2)	3.4 (±0.9	1.9	–179	+124	–206	–2056
PN4	+22.6 (±2.0)	9.1 (±0.6)	2.0 (±0.3)	1.7	–133	+123	–83	–1169

$\langle\Omega\rangle$ is the helix crossing angles, averaged over the last 10 ps of the MD trajectory, and over all adjacent helices of a bundle; $\langle D\rangle$ is the corresponding average of the helix-helix interaxial distance. $\langle R^{PORE}\rangle$ is the pore radius, averaged over the length of the pore. The values of $\langle R^{PORE}\rangle$, R_{MIN}, ΔE_{HH}^{VDW}, etc. all refer to the final structure from the corresponding MD simulations

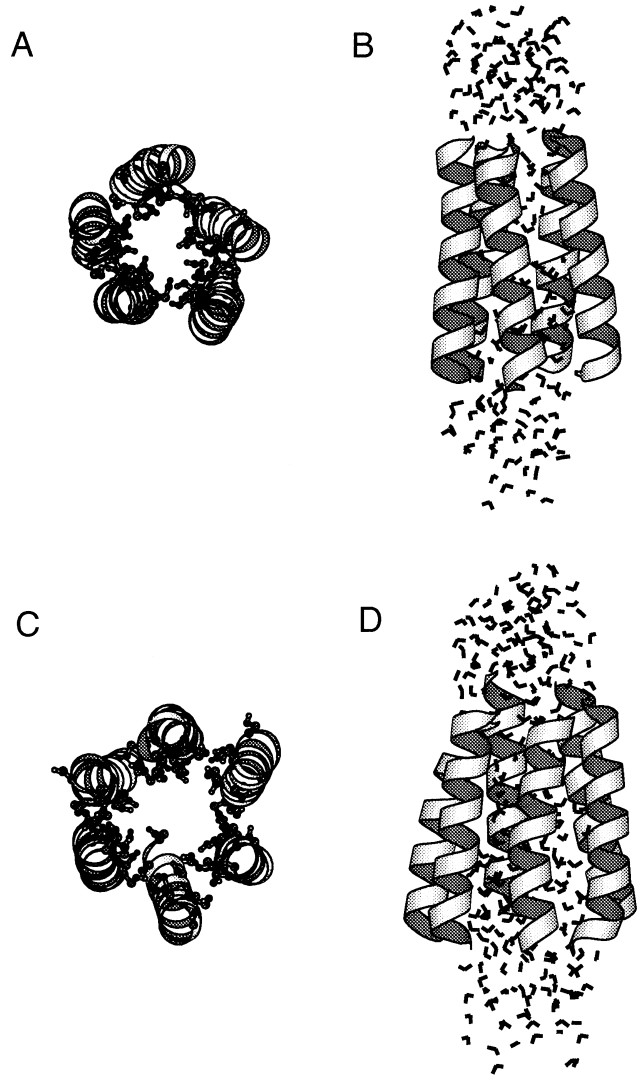

Fig. 1 A–D *IN5* and *IN6* model pores. Molscript (Kraulis 1991) generated diagrams of models *IN5* and *IN6*. In **A** and **C** the models are viewed down the pore (*z*) axis, with the serine sidechains shown in ball-and-stick fashion, and the polypeptide backbones as helical ribbons. In **B** and **D** the models are viewed perpendicular to the *z*-axis, with the N-termini of the helices at the bottom and the C-termini at the top of the diagram. The water molecules within and at the mouths of the pore are shown in bond fashion (i. e. as "V" shapes)

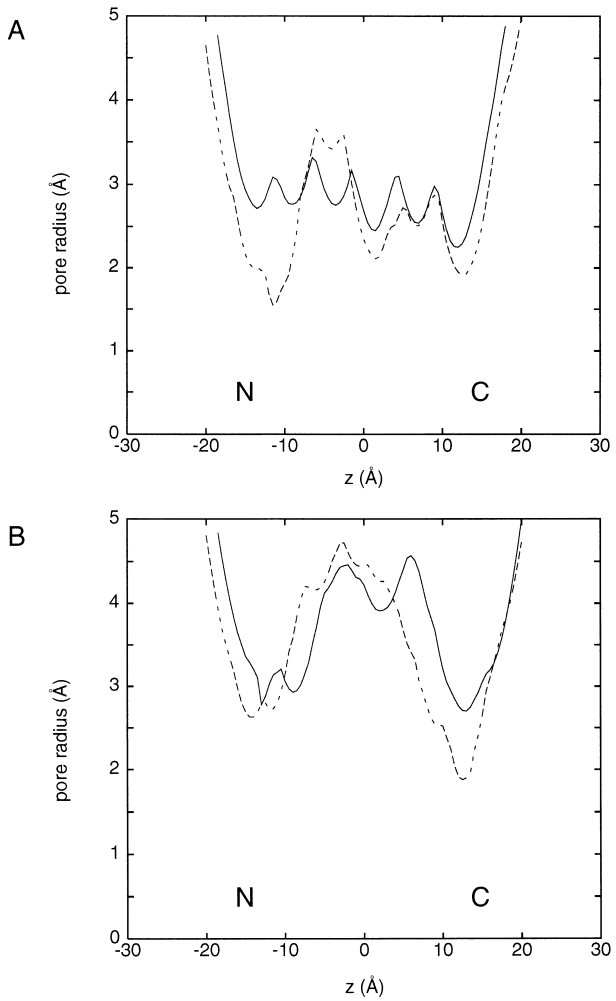

Fig. 2 A, B *IN5* and *IN6* pore radius profiles, calculated using HOLE (Smart et al. 1993). In each case the pore radius is displayed as a function of the position along the *z* (i. e. pore) axis. In **A** the pore radius profiles of *IN5* (*broken line*) and *IN6* (*solid line*) are shown at the start (i. e., $t = 0$ ps) of the MD simulations; in **B** the profiles for the same two models are shown at the end ($t = 100$ ps) of the MD simulations

Table 3 Model pores: water properties

Model	Zone	N_W	D ($Å^2\ ps^{-1}$)	τ_2^{-1} (ps^{-1})	μ (D)
Bulk water (experimental)	–	–	0.23 [1]	0.52 [2]	–
Bulk water (modified TIP3P)	all	231	0.32 (±0.12)	0.64 (±0.28)	–0.02 (±1.45)
IN4	Cap-N	34	0.29 (±0.20)	0.15 (±0.09)	–1.57 (±0.84)
	Pore	23	0.02 (±0.02)	0.08 (±0.13)	+1.32 (±1.33)
	Cap-C	46	0.24 (±0.12)	0.37 (±0.17)	–0.68 (±1.47)
IN5	Cap-N	55	0.32 (±0.27)	0.24 (±0.17)	–1.05 (±1.06)
	Pore	76	0.06 (±0.05)	0.07 (±0.05)	+1.94 (±0.82)
	Cap-C	78	0.31 (±0.14)	0.45 (±0.22)	–0.48 (±1.48)
IN6	Cap-N	63	0.36 (±0.26)	0.30 (±0.19)	–0.93 (±1.22)
	Pore	108	0.08 (±0.06)	0.08 (±0.04)	+1.74 (±0.74)
	Cap-C	85	0.28 (±0.14)	0.44 (±0.27)	–0.29 (±1.48)
*IN6**	Cap-N	68	0.17 (±0.14)	0.19 (±0.17)	–0.92 (±1.22)
	Pore	104	0.06 (±0.05)	0.03 (±0.03)	+1.84 (±0.72)
	Cap-C	84	0.20 (±0.11)	0.44 (±0.26)	–0.25 (±1.46)
PN4	Cap-N	53	0.26 (±0.17)	0.25 (±0.19)	–1.70 (±0.73)
	Pore	35	0.05 (±0.02)	0.07 (±0.06)	+1.97 (±0.55)
	Cap-C	57	0.23 (±0.11)	0.36 (±0.17)	–0.31 (±1.43)

Zones: Cap-N($z < -15$ Å) and Cap-C ($z > +15$ Å) = N- and C-terminal caps; Pore ($|z| < 15$ Å) = pore. N_W is the number of water molecules in a zone; D is their self diffusion coefficient; τ_2^{-1} is the second order rotational reorientation rates; and μ_z is the projection of the water molecule dipole onto the pore (i. e. z) axis. All values are given as mean (±SD) for all water molecules in a zone. Two sets of parameters are given for "bulk" water: experimental values ([1] – (Eisenberg and Kauzmann 1969); [2] – (Rahman and Stillinger 1971)); and values for a simulation of 231 modified TIP3P waters in a $(19.042)^3$ $Å^3$ box of water, using periodic boundaries. *IN6** refers to the repeat of the *IN6* simulation using the SHAKE option in CHARMM

it is evident that: (a) the overall geometry of the helix bundles, with the majority of the serine sidechains pointing into the lumen of the pore, is retained during the MD simulation; and (b) the water molecules remains as a cap at either mouth plus a column of waters filling the lumen of the pore. Thus, despite the absence of an explicit lipid bilayer the essential features of the pore models remain intact during these (relatively short) MD simulations.

However, this is not to imply that the structures of the model pores remain static during the MD simulations. From visual examination of the trajectories, some degree of repacking of the helices occurs. It is therefore useful to examine the geometry of the helix bundles, averaged over the last 10 ps of the trajectories (Table 2). The interaxial separation of the helices ($\langle D \rangle$) is close to the average for interacting pairs of α-helices in globular proteins ($D = 9.4$ Å; (Chothia et al. 1981)). The helix-helix crossing angles ($\langle \Omega \rangle$) are indicative of a left-handed coiled coil, as was found in the initial models generated by *in vacuo* SA/MD. Thus, the favoured 'ridges-in-grooves' packing observed in earlier *in vacuo* studies (Kerr et al. 1994) has been preserved during the MD simulations in the presence of water molecules. As the same packing mode is observed *in vacuo* and in the presence of water, it seems unlikely that this would be perturbed greatly by the presence of a fluid lipid bilayer. A similar mode of packing has been proposed on the basis of modelling and energy minimization studies by DeGrado and colleagues (Åkerfeldt et al. 1993).

It is also instructive to examine the potential energies of e. g. the structures at the end of the MD simulations (Table 2). The helix-helix interaction energies for both *IN5* and *IN6* reveal favourable van der Waals interaction, reflecting efficient packing of sidechains at the helix-helix interface, but have unfavourable electrostatic components. The latter result from repulsion of the parallel helix dipoles and of the positive charges at the unblocked N-termini of the helices. However, for both *IN5* and *IN6* the marginally favourable (ca. –50 kcal/mol) helix-helix interactions are overshadowed by highly favourable (ca. –2000 kcal/mol) pore-water interactions, which are in term dominated by their electrostatic component. This reflects the water-sidechain (ca. –1400 kcal/mol) and water-backbone (ca. –500 kcal/mol) electrostatic interactions, both of which are favourable.

Some changes are induced by the presence of water molecules within the pore, as is evident if one compares the dimensions of the pore *per se* at the start ($t = 0$ ps) and end ($t = 100$ ps) of the MD simulation. Examination of pore radius profiles reveals the nature of these changes. For model *IN5* (Fig. 2 A) the pore radius profile at the start of the simulation shows a regular pattern of maxima and minima reflecting the presence of 'rings' of pore-lining sidechains. This minimum pore radius is ca. 2.3 Å and the mean pore radius is ca. 2.8 Å over the length of the pore. At the end of the MD simulation the pore radius profile has become somewhat less regular, as might be expected. The average pore radius (Table 2) has not changed significantly,

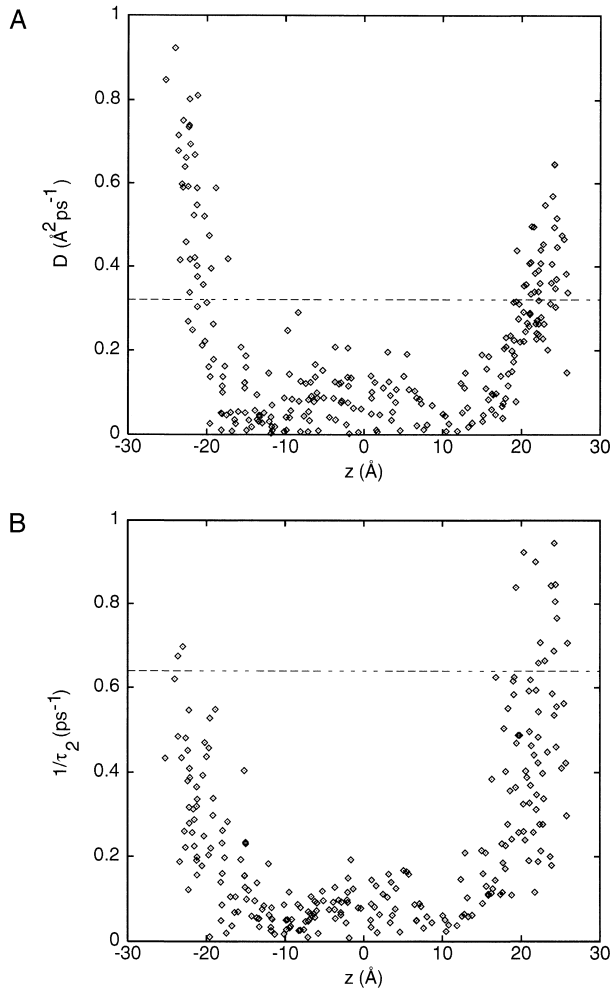

Fig. 3 A, B Analysis of water dynamics for simulation *IN6*. **A** Self-diffusion coefficient profile. The self-diffusion coefficient (*D*) is plotted for each water molecule as a function of the average water oxygen *z* coordinate for the trajectory. **B** Dipole reorientation rate profile. The second-order water dipole reorientation rate (τ_2^{-1}) is plotted for each water molecule as a function of the average water oxygen *z* coordinate for the trajectory. In both graphs the horizontal broken line indicates the corresponding average value of the parameter for the bulk water simulation (see Table 3)

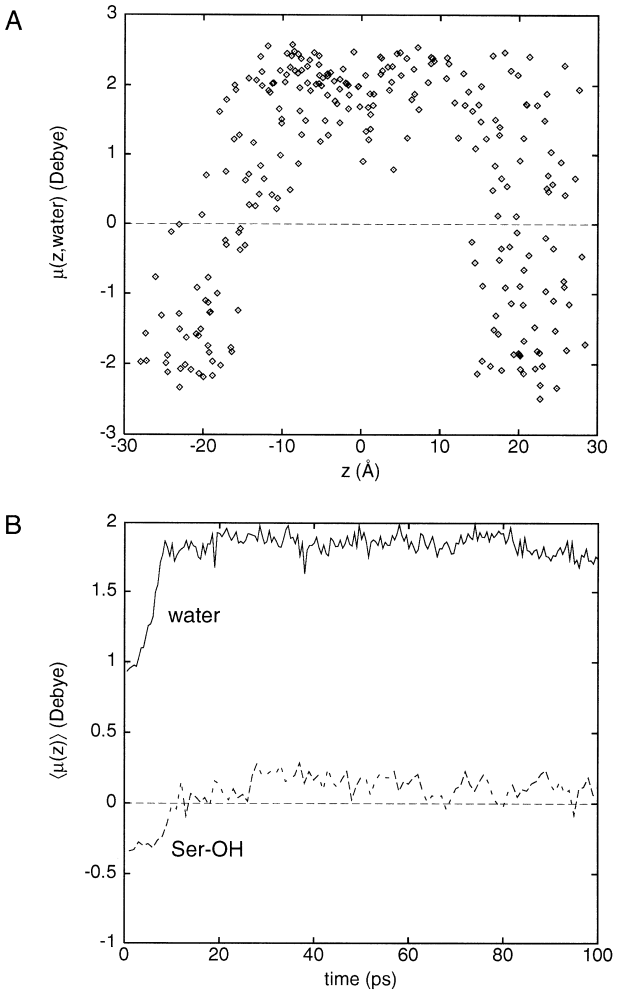

Fig. 4 A, B Analysis of orientation of water molecule dipoles in model *IN6*. **A** Water dipole orientation profile. The points represent μ_z for each water molecule, calculated from the structure at the end of the MD simulation, plotted as a function of the *z* coordinate of the water oxygen atom. In **B** the trajectories of the *z*-axis projections of the mean dipole moments of water molecules within the pore (*solid line*) and of the serine hydroxyl groups (*dotted line*) are shown

but the minimum pore radius has dropped to 1.6 Å, with a constriction at either end of the pore reflecting some dynamic distortion of the termini of the helices. A similar pattern of changes is observed for model *IN6* (Fig. 2 B). Visual inspection of the trajectories suggests that the changes in pore radius are consistent with a degree of insertion of water from the caps into the pores. Thus at $t = 0$ ps the numbers of pore waters (defined as those for which $|z| < 15$ Å) are 64 and 89 for models *IN5* and *IN6* respectively. At $t = 100$ ps the corresponding numbers of waters are 76 and 108.

One may use a pore radius profile as the basis of an approximate calculation of an upper bound on the conductance of the corresponding channel (Sansom and Kerr 1995). For *IN5* and *IN6* models at the end of the MD simulation this yields $G_{UPPER} = 360$ pS and 570 pS (for 0.5 M KCl) respectively. These values are compatible with the experimentally determined conductance of 70 pS in 0.5 M KCl for the $(LSSLLSL)_3NH_2$ channel (Lear et al. 1988). In similar calculations on porins (Sansom and Kerr 1995) it was noted that G_{UPPER} was ca. 5× higher than the experimental conductance. Applying a correction factor of 0.2 to the estimates of G_{UPPER} for *IN5* and *IN6* yields estimates of 70 and 110 pS respectively for the channel conductance. Of course, such calculations are somewhat approximate, but they do suggest that the models are in agreement with the experimental data. Note also that the major conductance exhibited by this channel has been estimated to correspond to a cutoff radius of ca. 4 Å (Lear et al. 1988), consistent with the value of $\langle R^{PORE} \rangle = 3.4$ (±0.9) Å for model *IN6*.

A major aim of our simulations is to examine the translational and rotational dynamics of water molecules within the lumen of the model pores. If water molecules are classified, on the basis of their time-averaged O atom coordinates, as being either cap ($|z| < 15$ Å) or pore ($|z| < 15$ Å) waters then a clear difference in dynamic behaviour emerges (Table 3). For both *IN5* and *IN6* the self-diffusion coefficient, *D*, of the cap waters does not differ significantly from that of bulk TIP3P water ($D = 0.32$ Å^2 ps^{-1}), whereas D for the pore waters is significantly depressed (by a factor of 0.2 for *IN5* and by a factor of 0.25 for *IN6*) relative to the bulk. This reduction in mobility of pore waters is also observed if one examines the rotational relaxation rate τ_2^{-1}. Plots of D and of τ_2^{-1} as a function of the time-averaged *z*-coordinate of the water molecule (Fig. 3) reveal this difference between pore and cap very clearly. From such graphs (that for *IN5*, not shown, is essentially the same) it is evident that confinement of waters within the pore significantly reduces their mobility. Detailed examination reveals a correlation between the mobility as a function of *z* (Fig. 3) and the pore radius profiles (Fig. 2). Thus, for *IN6*, the region of lowest mobility within the pore corresponds to the constriction at its C-terminal mouth (i. e. *z* ca. +10 Å).

One may also examine the structure of water within the model pores. As in previous simulations of hydrophobic helix bundles (Breed et al. 1996), the waters within the *IN5* and *IN6* pores align such that their dipoles are antiparallel to those of the α-helix backbones, the latter running from positive to negative *z* (Table 3 and Fig. 4 A). At the N-terminal cap of the pore the water dipoles are additionally aligned by the positively charged N-termini of the helices; at the C-terminal cap the water dipoles adopt more random orientations. If one examines the trajectory of the mean dipole moment of the waters within the pore (Fig. 4 B) it can be seen that alignment relative to the pore (*z*) axis is established within the first 10 ps of the simulation, and is maintained throughout. One may also examine the corresponding trajectory of the mean dipole of the serine sidechain OH groups. This reveals a small, but consistent, alignment of the SerOH dipoles anti-parallel to the helix dipoles, and thus parallel to the water dipoles. This is discussed in more detail in relation to model *PN4* (see below).

In order to examine the influence of the simulation conditions upon the behaviour of the water molecules, simulation *IN6* was repeated (as simulation *IN6**) with the SHAKE option activated. This keeps bonds lengths fixed and also has the effect of making the water molecules rigid, as in the unmodified TIP3P water model. As can be seen from Table 3, there are some changes in the absolute values of the self-diffusion coefficient and the rotational reorientation rate of the water, as would be expected with a change in water parameters. However, the overall pattern of a reduction in rotational and translational dynamics of water within the pore relative to the caps is retained. Thus, for *IN6 D(cap)/D(pore)* is ca. 4 whereas for *IN6** the corresponding value is ca. 6. If one plots either *D* or τ_2^{-1} *vs. z* for *IN6** (graph not shown) then the resultant profiles along the length of the pore are very similar to those for *IN6* (Fig. 3). As is also evident from Table 3, the alignment of the water dipole relative to the helix dipoles is the same for *IN6** as for *IN6*.

Model *PN4* vs. Model *IN4*

A comparison of models *PN4* and *IN4* was made in order to investigate possible reasons why the peptide $(LSLLLSL)_3NH_2$ forms H^+ selective channels (as opposed to the monovalent cation selective channels formed by $(LSSLLLSL)_3NH_2$; (Lear et al. 1988)). DeGrado and colleagues, using *in vacuo* model building and energy minimization (Lear et al. 1988; Åkerfeldt et al. 1993) have suggested that in going from $(LSLLLSL)_3NH_2$ to $(LSSLLSL)_3NH_2$ the loss of one serine residue per heptad repeat preferentially stabilizes a tetrameric helix assembly and that, furthermore, a pore formed by a tetrameric bundle is only wide enough to allow H^+ to permeate. We therefore wished to compare the pore dimensions in the *PN4* and *IN4* models. It should be stressed that the *IN4* model is included for comparative purposes – the experimental results (Lear et al. 1988) suggest that it is not a major channel species. The starting model for *IN4* was generated by SA/MD in the same way as for *IN5* and *IN6*. The starting model for *PN4* was obtained by taking that for *IN4* and using Quanta to replace the three serine sidechains by leucine sidechains.

Snapshots of the two models are shown in Fig. 5, and details of the bundle geometries and energetics are summarized in Table 2. From the latter it is evident that both *PN4* and *IN4* exhibit a more positive crossing angle (Ω ca. +23°) than either *IN5* or *IN6* (Ω ca. +12°). This indicates a greater degree of supercoiling of the helices within tetrameric than within pentameric or hexameric assemblies. In model *IN4* the interhelix separation ($\langle D \rangle = 8.3$ Å) is significantly lower than for *PN4*. This is accompanied by a marginally favourable ΔE_{HH}^{ELEC} for *IN4*, suggesting that inter-helix H-bonds formed by interfacial serine residues just outweigh the repulsive dipole/dipole interactions between adjacent helices of the bundle.

Examination of snapshots of the two models (Fig. 5 A, B) at $t = 0$ ps and $t = 100$ ps reveals significant differences between the behaviour of *PN4* and *IN4*. In both models, at $t = 0$ ps the pore is discontinuous, i. e. the network of water/water H-bonds is broken in several places. This is in agreement with our earlier suggestion (Kerr et al. 1994) that, in general, tetrameric helix bundles form a pores which are too narrow to support ion permeation. This remains the case for *IN4* throughout the simulation, even though a few (ca. 7) additional water molecules enter the N-terminal mouth of the pore. In contrast, in *PN4* at an early stage during the simulation (t <50 ps) ca. 20 additional water molecules enter the pore. This results in formation of a continuous H-bonded column of water from end to end of the *PN4* bundle. The consequences of this difference between *PN4* and *IN4* in terms of pore radius profiles are illustrated in Fig. 5 C, D. For *IN4* (Fig. 5 C) there is no significant change in the pore radius profile dur-

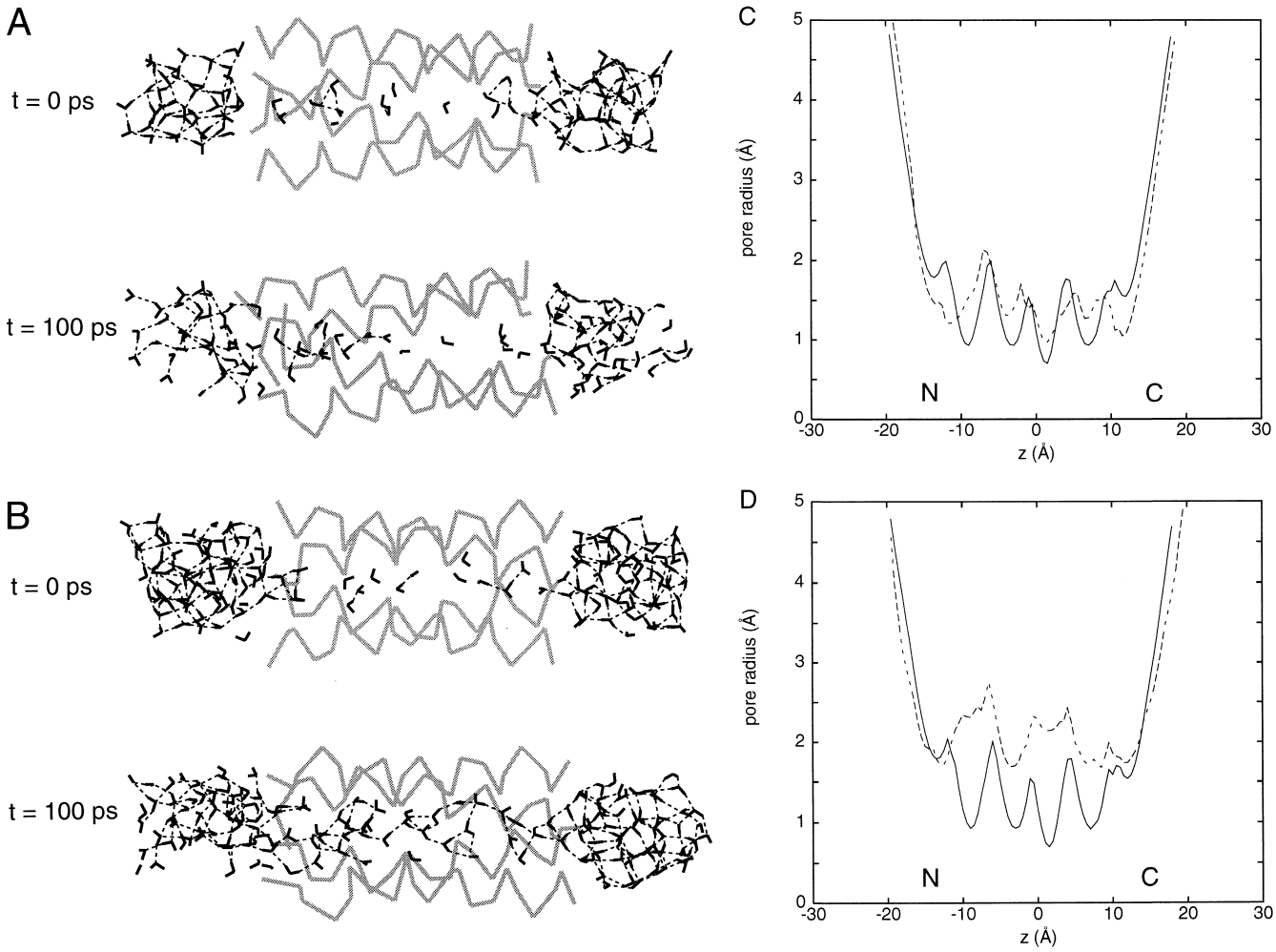

Fig. 5 Comparison of the (**A**) *IN4* and (**B**) *PN4* models. For each model the structure at the start ($t = 0$ ps) and end ($t = 100$ ps) of the MD simulation is shown. The helices are shown as Cα traces (in grey). The water molecules are shown in bonds fashion in black, with *dotted lines* corresponding to water-water H-bonds. The corresponding pore radius profiles for (**C**) *IN4* and (**D**) *PN4* are shown, with the *dotted lines* representing the profiles for the $t = 0$ ps structures and the *solid lines* the profiles for the $t = 100$ ps structures

ing the 100 ps simulation. In contrast, for *PN4* (Fig. 5 D) the radius increases significantly along the entire length of the pore. Thus, for $t = 90$ to 100 p (Table 2), the mean pore radius for *IN4* is 1.5 Å whereas that for *PN4* is 2.0 Å. More significantly, the *minimum* pore radius increases from 0.97 Å to 1.7 Å. In combination with the analysis of helix/helix and pore/water interaction energies that suggests that in *IN4* the additional serine residues form favourable electrostatic interactions at the helix interfaces which resist entry of additional water molecules, thus maintaining a narrow, *discontinuous* pore. In contrast, in *PN4* the absence of such H-bonding interactions at the helix-helix interfaces allows the bundle to expand slightly, giving rise to a continuous water-filled pore.

The pore radius profile may be used to calculate a value of $G_{UPPER} = 760$ pS for *PN4* at $t = 100$ ps, estimated using a resistivity of 0.047 Ωm for 0.5 M HCl (Hille 1992). The experimental conductance for $(LSLLLSL)_3NH_2$ channels is 120 pS in 0.5 M HCl (Lear et al. 1988; DeGrado and Lear 1990; Lear et al. 1994). If one applies the correction factor of 0.2 discussed above to the value of G_{UPPER}, one obtains an estimate of 150 pS for the conductance of *PN4*, i. e. close to the experimental value. It must be stressed that this is a rather approximate calculation of the conductance expected on the basis of a model, and that the approximation is expected to be worse for H^+ ions than for other ionic species. However, the agreement between prediction and experiment is encouraging.

The dynamics of water molecules within *PN4* and *IN4* are compared in Table 3. The same general pattern is seen as for the previous two models, namely a reduction in mobility of water molecules within the pore lumen. The mobility of pore waters is lower within tetrameric bundles than in pentameric and hexameric bundles, as might be anticipated. In the case of the discontinuous pore of *IN4* the mobility is almost as low as that of the single file of water molecules observed in simulations of gramicidin A ($D = 0.0003$ Å^2 ps^{-1}; (Roux and Karplus 1994)).

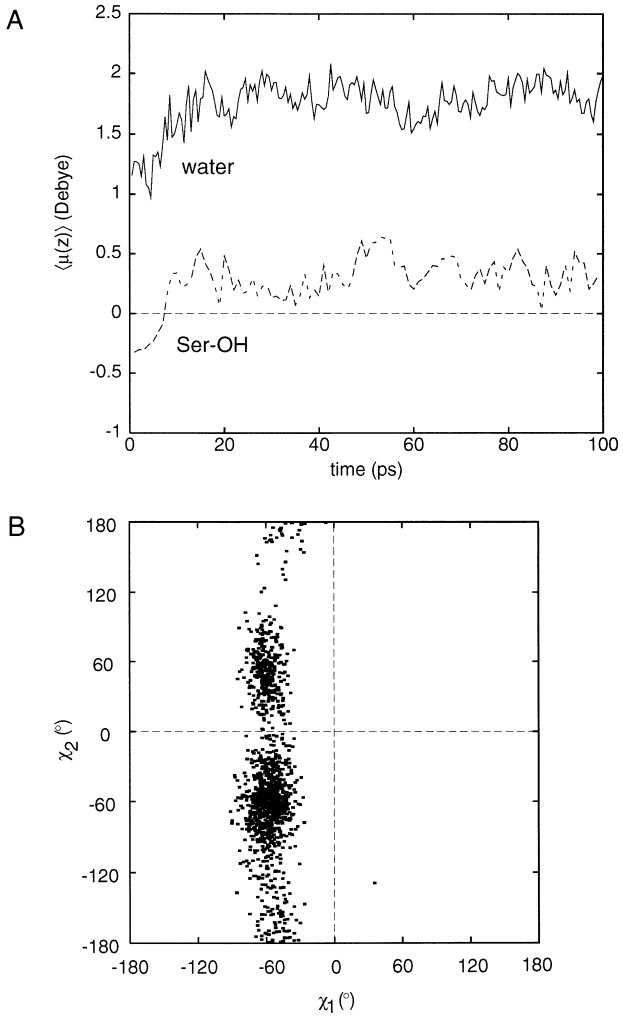

Fig. 6 A, B Analysis of orientation of water molecule and serine hydroxyl dipoles in model *PN4*. In **A** the trajectories of the *z*-axis projections of the mean dipole moments of water molecules within the pore (*solid line*) and of the serine hydroxyl groups (*dotted line*) are shown. In **B** the distribution of (χ_1, χ_2) values, defining the serine sidechain conformations, is shown. Each point represents a single serine sidechain, with snapshots taken every 1 ps from $t = 50$ ps to 100 ps during the trajectory

Table 4 Polarization of water and hydroxyls

Model	$\langle \mu_z$ (water, pore)$\rangle$ (Debye)	$\langle \mu_z$ (SerOH)$\rangle$ (Debye)
IN4	+1.49 (±0.12)	+0.06 (±0.08)
IN5	+1.87 (±0.06)	+0.26 (±0.09)
IN6	+1.84 (±0.07)	±0.11 (±0.07)
PN4	+1.79 (±0.13)	+0.36 (±0.13)

$\langle \mu_z$(water, pore)$\rangle$ is the average *z*-projection of the dipoles of water molecules within the pore; $\langle \mu_z$(SerOH)$\rangle$ is the average *z*-projection of the dipoles of serine hydroxyl groups. In both cases the average is across structures saved every 1 ps from $t = 50$ to 100 ps of the simulations. $\langle \mu_z$(SerOH, $t = 0$)$\rangle$ is the average z-projection of the dipoles of serine hydroxyl groups at the start of the MD simulation

The alignment of the water and SerOH dipoles relative to the pore axis observed in *IN5* and *IN6* is also observed in *IN4* and *PN4* (Table 4). Let us examine the situation in *PN4* in more detail. From Table 4 it is evident that the water dipoles are aligned largely antiparallel to the helix dipoles within the lumen of the pore. Furthermore, the degree of alignment of the SerOH dipoles is greatest for *PN4*, indicating a polarized network of water-water and water-sidechain H-bonds within the pore. The trajectories of the water and SerOH dipoles (Fig. 6 A) indicate that this alignment is established within less than 20 ps and is then maintained throughout the duration of the simulation. If one calculates the *total* dipole moment then that of the protein (projected on *z*) is –443 Debye (where a positive dipole points from the N-termini to the C-termini). Within the pore, the water molecules oppose this by +78 Debye and the serine sidechains by +32 Debye. Thus the effect of the orientation of the serine sidechains is about 50% that of the pore waters. The alignment of the serine sidechains may be characterized in terms of their χ_1 and χ_2 torsion angles. As discussed by Gray and Matthews (1984) a value of $\chi_1 = -60°$ allows a serine sidechain to H-bond back to the mainchain carbonyl oxygen of residue *i*–4 within an α-helix. Examination of the trajectories reveals that χ_1 ca. –60° is maintained throughout, with only occasional brief (less than 5 ps) transitions, which are mainly to χ_1 ca. +60°, which also allows such sidechain/mainchain H-bonds to be formed. Examination of the initial, *in vacuo*, model revealed that nearly all possible SerOH-carbonyl O(*i*–4) H-bonds were formed. However, examination of the χ_2 values reveals rather subtle behaviour in the presence of water. By construction of idealized models one may readily demonstrate that conformation (χ_1, χ_2) = (–60°, +60°) allows formation of a SerOH to mainchain CO H-bond (as discussed above), whereas conformation (χ_1, χ_2) = (–60°, –60°) breaks this H-bond and aligns the SerOH dipole in the positive direction along *z*, as seen in the MD simulation. In Fig. 6 B the distribution of (χ_1, χ_2) values for all serine residues during the latter half of the simulation is shown. It clear that (χ_1, χ_2) = (–60°, –60°) is the most populated conformation. The relationship between this sidechain conformation and the alignment of the water and SerOH dipoles relative to the helix dipoles is summarized in Fig. 7.

Discussion

Evaluation of methology

Three main aspects of the methodology require evaluation: (a) the assumptions underlying the models; (b) initial generation of the models via *in vacuo* SA/MD; and (c) MD simulations in the presence of water within and at the mouths of the model pores.

The assumptions embodied in the models presented are that: (a) the peptides adopt an α-helical conformation; (b) the resultant α-helices associate within lipid bilayers as approximately parallel transbilayer bundles; and (c)

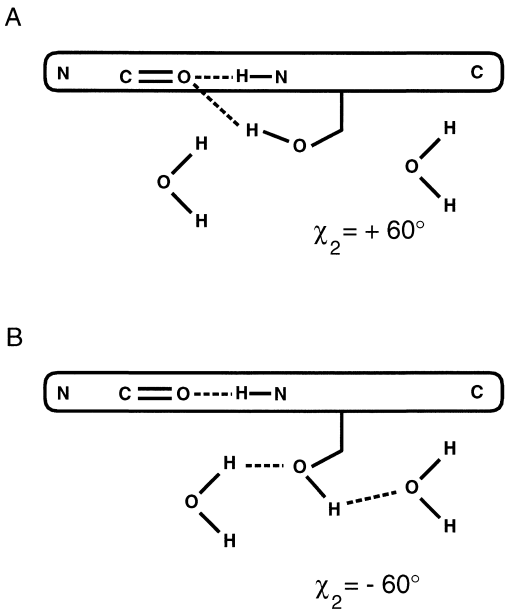

Fig. 7 A, B Cartoon of the factors influencing the conformation of a serine sidechain within a helix bundle. For clarity only a single helix is shown (as an *elongated box*). The two alternative conformations possible in the MD simulations with water is present are shown, with H-bonding either **A** "back" to the mainchain carbonyl or **B** "forward" to an intra-pore water molecule, the latter being oriented by the α-helix dipoles forming the lining of the pore. In the latter case extended networks of water-SerOH-water may be formed

within bundles the helices are oriented such that the serine siedechains line the pore. DeGrado and colleagues (DeGrado and Lear 1990) have presented CD which support the α-helical conformation of these peptides. The main evidence in favour of a parallel packing mode for the helices arises from the voltage asymmetry of channel formation (Lear et al. 1988) and from the rectification properties of the resultant channels (Kienker et al. 1994). The assumption that the serine sidechains form the pore lining is primarily on energetic grounds. It is highly unlikely that a bundle of amphipathic helices spanning a lipid bilayer would form with the serine sidechains facing outward. This would form an assembly with hydrophilic exterior exposed to the acyl chains of the lipid molecules.

Initial pore models were generated by *in vacuo* SA/MD calculations. This method has been previously demonstrated to yield plausible models of pores formed by parallel α-helix bundles (Kerr et al. 1994), and has also been applied to models of seven transmembrane helix bundles (Sansom et al. 1995) and to pores formed by anti-parallel β-barrels (Sansom and Kerr 1995). In the absence of high resolution structures for trans-bilayer pores formed by synthetic CFPs one remains uncertain of the extent to which such models are correct. However, the models presented for amphipathic helix bundles are supported by a spectroscopic evidence for their secondary structure (see above) plus indirect evidence for the overall architecture of the bundles (Sansom 1991; Sansom 1993). The other limitation of the models is the absence of a lipid bilayer. Inclusion of an all-atom model for a bilayer would have rendered the computations somewhat lengthy, and may not be justified at this stage. However, as the direct interactions of the water molecules are with one another and with the protein atoms lining the pore, omission of a lipid bilayer is an acceptable first approximation.

MD simulations in the presence of pore water molecules were carried out using a similar protocol to that employed in other studies of water in ion channels, both by us (Breed et al. 1996) and by other investigators (Chiu et al. 1991; Roux and Karplus 1994; Engels et al. 1995). Two aspects require consideration: the water model employed, and the effect of the restraints applied during the MD simulations. We used the modified TIP3P model in CHARMM, similar to that which has been used in a number of other simulation studies (Roux and Karplus 1991; Knapp and Muegge 1993; Komeiji et al. 1993; Venable et al. 1993). Although the values of D and τ_2^{-1} for a bulk TIP3P simulation do not agree exactly with the experimental values for these parameters (Table 3) the disagreement is not so great as to invalidate the current study. It seems unlikely that an alternative water model would radically transform the overall patterns in dynamic behaviour and structure of pore water which are observed. This is supported by the results of simulation *IN6**, with SHAKE applied during the simulations, which yielded similar water behaviour to the corresponding simulation *IN6*.

During the MD simulations weak cylindrical restraints were imposed on the water molecules, coming into play mainly at the cap regions, and intended to prevent "evaporation" at the ends of the pore. It was wondered whether such restraints might not be responsible for the greater mobility of the water molecules in those regions. That this is not the case was supported by simulations of water molecules in the presence of such restraints but in the absence of any protein (Sansom et al. 1995) which do not increase the mobility of the cap waters.

A further possible concern of these simulations is that 100 ps is a relatively short simulation time. Although this is true, it seems to be sufficient to capture the difference in dynamics between pore and cap water. For example, in a previous study of simple hydrophobic helix bundles (Breed et al. 1996) comparison of water dynamics for a 100 ps and a 500 ps simulation did not reveal any significant difference. Similar results have been obtained by comparing 100 ps and 500 ps simulations of water within models of the pore formed by the simple Ca^{2+} permeable channel phospholamban (Sansom et al., unpublished results). Overall, these and other test simulations suggest that whilst the current simulations doubtless represent only a first approximation to the behaviour of channels formed by these amphiphatic helical peptides, they are sufficiently accurate to merit further analysis.

Implications of results

The simulations of models *IN5* an *IN6* are in agreement with simulations of other channel systems in suggesting

that water within the pore region differs in its structural a dynamic properties from bulk water. This has now been suggested to be the case in simulations of simple hydrophobic pores (Breed et al. 1996), in gramicidin (Chiu et al. 1991; Roux and Karplus 1994), in peptide nanotubes (Engels et al. 1995), in alamethicin helix bundles (Breed et al. 1996) and, here, in *de novo* designed peptide channels. This suggests that this may be a general result applicable to a wide range of ion channels. Indeed, preliminary simulation results (Smith and Sansom, unpublished results) suggests that such perturbations of water properties within pores may also apply to the transmembrane channel domain of the nicotinic acetylcholine receptor (Sansom et al. 1995; Sankararamakrishnan et al. 1996). A novel feature of the channels discussed in the current paper is that in addition to alignment of the water dipoles within the pore, a degree of alignment of the sidechain dipoles also occurs. This is discussed in more detail below.

The comparison of models *IN4* and *PN4* is quite illuminating. It had previously been suggested that the additional serine sidechain at the helix/helix interface in model *IN4* destabilized the tetrameric bundle at the expense of higher order bundles of $(LSSLLSL)_3NH_2$ (Lear et al. 1988; Lear et al. 1994). Our simulations suggest that the situation is more complex than this. Comparing models *IN4*, *IN5* and *IN6*, calculations of the potential energies of helix/helix interactions (Table 2) suggest that *in vacuo* one would expect *IN4* to form the most stable assembly. However, in the presence of water the greater degree of exposure of serines within the pore makes the pentameric and hexameric assemblies more favoured, as may be seen from the pore/water interaction energies. This explains the formation of higher conductance channels, enabling permeation of a range of monovalent cations, being formed by $(LSSLLSL)_3NH_2$ (Lear et al. 1988; Åkerfeldt et al. 1993).

The formation of exclusively H^+ selective channels by $(LSLLLSL)_3NH_2$ (Lear et al. 1988; DeGrado and Lear 1990; Åkerfeldt et al. 1993) is more difficult to explain. Analysis of model *PN4* indicates that upon hydration the pore is wide enough to permit water molecules, and possibly partially dehydrated metal cations, to pass. It may be a more subtle explanation than simply the dimensions of the pore must be sought. To understand why model *PN4* does not allow eg. K^+ ions (ionic radius 1.3 Å) to permeate it may be necessary to consider in detail the free energy profile of an ion as it passes through the model pore. When such calculations have been performed for e. g. gramicidin (Roux and Karplus 1994; Dorman et al. 1996) they reveal quite subtle energetic effects which must be taken into account if one is to understand ion selectivity. In particular, it is possible that alignment of the water and serine OH dipoles within the pore, which is pronounced in *PN4*, may play a role in the observed high H^+ conductance. Figure 7 suggests how the cooperative water/serine interactions might prime the channel for H^+ 'hopping'.

In addition to their importance for channels formed by peptides, these simulations may have broader implications for more complex membrane transport proteins. In particular, the reduced mobility and 'structuring' of water within narrow pores (as exemplified by *PN4*) may, on the basis e. g. of studies of gramicidin (Roux and Karplus 1994), be relevant to H^+ transport proteins, such as bacteriorhodopsin (Fischer et al. 1994; Kandori et al. 1995), cytochrome oxidase (Iwata et al. 1995), and the mitochondrial F-ATPase (Abrahams et al. 1994). Our studies reinforce this proposal, and also suggest that one should take into account the coupled interactions of pore water and pore-lining sidechain conformation in order to understand possible H^+ transport pathways. In particular, our studies suggest that one should consider the effects of strong local electrostatic fields, whether generated by backbone dipoles (as here) or by charged sidechains, on the orientation of water and polar sidechains which may form 'wires' for conduction of protons.

These simulations are currently being extended in two directions. Models of CFPs are being employed in simulations of the energetics of ion permeation in order to better understand the nature of ion selectivity. In parallel, the MD procedures employed in the current study are being used to investigate models of 'simple' proton channels proteins, such as the M2 protein of influenza A virus (Sansom and Kerr 1993).

Acknowledgements This work was supported by the Wellcome Trust. Our thanks to our colleagues (Dr. I. Kerr, Dr. G. Smith, Dr. O. Smart, Dr. J. Breed, Mr. H. Son, Mr. P. Biggin, Mr. P. la Rocca and Miss C. Adcock) for their interest in and help with this work, and to the Oxford Centre for Molecular Science for computational facilities.

References

Abrahams JP, Leslie AGW, Lutter R, Walker JE (1994) Structure at 2.8 Å resolution of F1-ATPase from bovine heart mitochondria. Nature 370: 621–628

Adams PD, Arkin IT, Engelman DM, Brünger AT (1995) Computational searching and mutagenesis suggest a structure for the pentameric transmembrane domain of phospholamban. Nature Struct Biol 2: 154–159

Åkerfeldt KS, Kim RM, Camac D, Groves JT, Lear JD, DeGrado WF (1992) Tetraphilin: a four-helix proton channel built on a tetraphenylporphyrin framework. J Am Chem Soc 114: 9656–9657

Åkerfeldt KS, Lear JD, Wasserman ZR, Chung LA, DeGrado WF (1993) Synthetic peptides as models for ion channel proteins. Acc Chem Res 26: 191–197

Arkin IT, Rothman M, Ludlam CFC, Aimoto S, Engelman DM, Rothschild KJ, Smith SO (1995) Structural model of the phospholamban ion channel complex in phospholipid membranes. J Mol Biol 248: 824–834

Breed J, Sankararamakrishnan R, Kerr ID, Sansom MSP (1996) Molecular dynamics simulations of water within models of transbilayer pores. Biophys J 70: 1643–1661

Brooks BR, Bruccoleri RE, Olafson BD, States DJ, Swaminathan S, Karplus M (1983) CHARMM: A program for macromolecular energy, minimisation, and dynamics calculations. J Comp Chem 4: 187–217

Brünger AT (1992) X-PLOR Version 3.1. A system for X-ray crystallography and NMR Ct, Yale University Press

Chiu SW, Jakobsson E, Subramanian S, McCammon JA (1991) Time-correlation analysis of simulated water motion in flexible and rigid gramicidin channels. Biophys J 60: 273–285

Chothia C, Levitt M, Richardson D (1981) Helix to helix packing in proteins. J Mol Biol 145: 215–250

Chung LA, Lear J, DeGrado WF (1992) Fluorescence studies of the secondary structure and orientation of a model ion channel peptide in phospholipid vesicles. Biochemistry 31: 6608 – 6616

Cowan SW, Schirmer T, Rummel G, Steiert M, Ghosh R, Pauptit RA, Jansonius JN, Rosenbusch JP (1992) Crystal structures explain functional properties of two *E. coli* porins. Nature 358: 727 – 733

Dani JA, Levitt DG (1990) Diffusion and kinetic approaches to describe permeation in ionic channels. J Theor Biol 146: 289 – 301

DeGrado WF, Lear JD (1990) Conformationally constrained α-helical peptide models for protein ion channels. Biopolymers 29: 205 – 213

Dorman V, Partenskii MB, Jordan PC (1996) A semi-microscopic Monte Carlo study of permeation energetics in a gramicidin-like channel: the origin of cation selectivity. Biophys J 70: 121 – 134

Eisenberg D, Kauzmann W (1969) The structure and properties of water. Oxford University Press, Oxford

Engel A, Walz T, Agre P (1994) The aquaporin family of membrane water channels. Curr Opin Struct Biol 4: 545 – 553

Engels M, Bashford G, Ghadiri MR (1995) Structure and dynamics of self-assembling peptide nanotubes and the channel-mediated water organization and self-diffusion. A molecular dynamics study. J Amer Chem Soc 117: 9151 – 9158

Fischer WB, Sonar S, Marti T, Khorana HG, Rothschild KJ (1994) Detection of a water molecule in the active-site of bacteriorhodopsin–hydrogen-bonding changes during the primary photoreaction. Biochem 33: 12 757 – 12 762

Gray TM, Matthews BM (1984) Intrahelical hydrogen bonding of serine, threonine and cysteine residues within α-helices and its relevance to membrane-bound proteins. J Mol Biol 175: 75 – 81

Hille B (1992) Ionic channels of excitable membranes, 2nd edn. Sinauer Associates Inc, Sunderland, Mass

Iwata S, Ostermeier C, Ludwig B, Michel H (1995) Structure at 2.8 Å resolution of cytochrome c oxidase from *Paracoccus denitrificans.* Nature 376: 660 – 669

Jorgensen WL, Chandresekhar J, Madura JD, Impey RW, Klein ML (1983) Comparison of simple potential functions for simulating liquid water. J Chem Phys 79: 926 – 935

Kandori H, Yamazaki Y, Sasaki J, Needleman R, Lanyi JK, Maeda A (1995) Water-mediated proton transfer in proteins – an FTIR study of bacteriorhodopsin. J Am Chem Soc 117: 2118 – 2119

Karshikoff A, Spassov V, Cowan SW, Ladenstein R, Schirmer T (1994) Electrostatic properties of two porin channels from *Escherichia coli.* J Mol Biol 240: 372 – 384

Kerr ID, Doak DG, Sankararamakrishnan R, Breed J, Sansom MSP (1996) Molecular modelling of Staphylococcal δ-toxin ion channels by restrained molecular dynamics. Prot Engng 9: 161 – 171

Kerr ID, Dufourcq J, Rice JA, Fredkin DR, Sanson MSP (1995) Ion channel formation by synthetic analogues of Staphylococcal δ-toxin. Biochim Biophys Acta 1236: 219 – 227

Kerr ID, Sankararamakrishnan R, Smart OS, Sansom MSP (1994) Parallel helix bundles and ion channels: molecular modelling via simulated annealing and restrained molecular dynamics. Biophys J 67: 1501 – 1515

Kienker PK, DeGrado WF, Lear JD (1994) A helical-dipole model describes the single-channel current rectification of an uncharged peptide ion channel. Proc Nat Acad Sci USA 91: 4859 – 4863

Knapp EW, Muegge I (1993) Heterogeneous diffusion of water at protein surfaces: application to BPTI. J Phys Chem 97: 11 339 – 11 343

Komeiji Y, Uebayasi M, Someya J, Yamato I (1993) A molecular dynamics study of solvent behaviour around a protein. Proteins Struct Func Genet 16: 268 – 277

Kraulis PJ (1991) MOLSCRIPT: a program to produce both detailed and schematic plots of protein structures. J Appl Cryst 24: 946 – 950

Kreusch A, Schulz GE (1994) Refined structure of the porin from *Rhodobacter blastica.* J Mol Biol 243: 891 – 905

Kuyucak S, Chung SH (1994) Temperature dependence of conductivity in electrolyte solutions and ionic channels of biological membranes. Biophys Chem 51: 15 – 24

Lear JD, Wasserman ZR, DeGrado WF (1988) Synthetic amphiphilic peptide models for protein ion channels. Science 240: 1177 –1181

Lear JD, Wasserman ZR, DeGrado WF (1994) Use of synthetic peptides for the study of membrane protein structure. Membrane protein structure: experimental approaches. Oxford University Press, Oxford

Mellor IR, Thomas DH, Sansom MSP (1988) Properties of ion channels formed by *Staphylococcus aureus* δ-toxin. Biochim Biophys Acta 942: 280 – 294

Montal M, Montal MS, Tomich JM (1990) Synporins-synthetic proteins that emulate the pore structure of biological ionic channels. Proc Natl Acad Sci USA 87: 6929 – 6933

Montal M (1995) Design of molecular function: channels of communication. Ann Rev Biophys Biomol Struct 24: 31 – 57

Oiki S, Madison V, Montal M (1990) Bundles of amphipathic transmembrane α-helices as a structural motif for ion conducting channel proteins: studies on sodium channels and acetylcholine receptors. Proteins: Struct Func Genet 8: 226 – 236

Raghunathan G, Seetharamulu P, Broosk BR, Guy HR (1990) Models of δ-hemolysin membrane channels and crystal structures. Proteins: Struct Func Genet 8: 213 – 225

Rahman A, Stillinger FH (1971) Molecular dynamics study of liquid water. J Chem Phys 55: 3336 – 3359

Rossky PJ, Karplus M (1979) Solvation. A molecular dynamics study of a dipeptide in water. J Amer Chem Soc 101: 1913 – 1936

Roux B, Karplus M (1991) Ion transport in a model gramicidin channel: structure and thermodynamics. Biophys J 59: 961 – 981

Roux B, Karplus M (1994) Molecular dynamics simulations of the gramicidin channel. Ann Rev Biophys Biomol Struct 23: 731 – 761

Sankararamakrishnan R, Adcock C, Sansom MSP (1996) The pore domain of the nicotinic acetylcholine receptor: molecular modelling and electrostatics. Biophys J 71 (4) (in press)

Sankararamakrishnan R, Sansom MSP (1995) Modelling packing interactions in parallel helix bundles: pentameric bundles of nicotinic receptor M2 helices. Biochim Biophys Acta 1239: 122 – 132

Sansom MSP (1991) The biophysics of peptide models of ion channels. Prog Biophys Mol Biol 55: 139 – 236

Sansom MSP (1993a) Alamethicin and related peptaibols- model ion channels. Eur Biophys J 22: 105 – 124

Sansom MSP (1993b) Structure and function of channel-forming peptaibols. Quart Rev Biophys 26: 365 – 421

Sansom MSP, Kerr ID (1993) Influenza virus M2 protein: a molecular modelling study of the ion channel. Prot Eng 6: 65 – 74

Sansom MSP, Kerr ID (1995) Transbilayer pores formed by β-barrels: molecular modelling of pore structures and properties. Biophys J 69: 1334 – 1343

Sansom MSP, Sankararamakrishnan R, Kerr ID (1995) Modelling membrane proteins using structural restraints. Nature Struct Biol 2: 624 – 631

Sansom MSP, Son HS, Sankararamakrishnan R, Kerr ID, Breed J (1995) Seven-helix bundles: molecular modelling via restrained molecular dynamics. Biophys J 68: 1295 – 1310

Smart OS, Goodfellow JM, Wallace BA (1993) The pore dimensions of gramicidin A. Biophys J 65: 2455 – 2460

Unwin N (1989) The structure of ion channels in membrane of excitable cells. Neuron 3: 665 – 676

Unwin N (1993) Nicotinic acetylcholine receptor at 9 Å resolution. J Mol Biol 229: 1101 – 1124

Unwin N (1995) Acetylcholine receptor channel imaged in the open state. Nature 373: 37 – 43

Venable RM, Brooks BR, Carson FW (1993) Theoretical studies of the relaxation of a monomeric subunit of HIV-1 protease in water using molecular dynamics. Proteins: Struct Func Genet 15: 374 – 384

Walz T, Typke D, Smith BL, Agre P, Engel A (1995) Projection map of aquaporin-1 determined by electron crystallography. Nature Struct Biol 2: 730 – 732

You S, Peng S, Lien L, Breed J, Sansom MSP, Woolley GA (1996) Engineering stabilized ion channels: covalent dimers of alamethicin. Biochem 35: 6225 – 6232